Composition below 10^{19}eV

US Auger Collaboration Meeting

Colorado State Univeristy

John A.J. Matthews

New Mexico Center for Particle Physics

University of New Mexico

February 28, 2003

1. What do we know?
2. We would like to know: f_p *versus* E
3. **And** over the largest ΔE
4. Energies below $\sim 10^{19}$eV implies hybrid:
   (a) ... to maintain experimental resolution
   (b) **and** below some energy hybrid is 100% of **the data**

1. Background (con't) ...

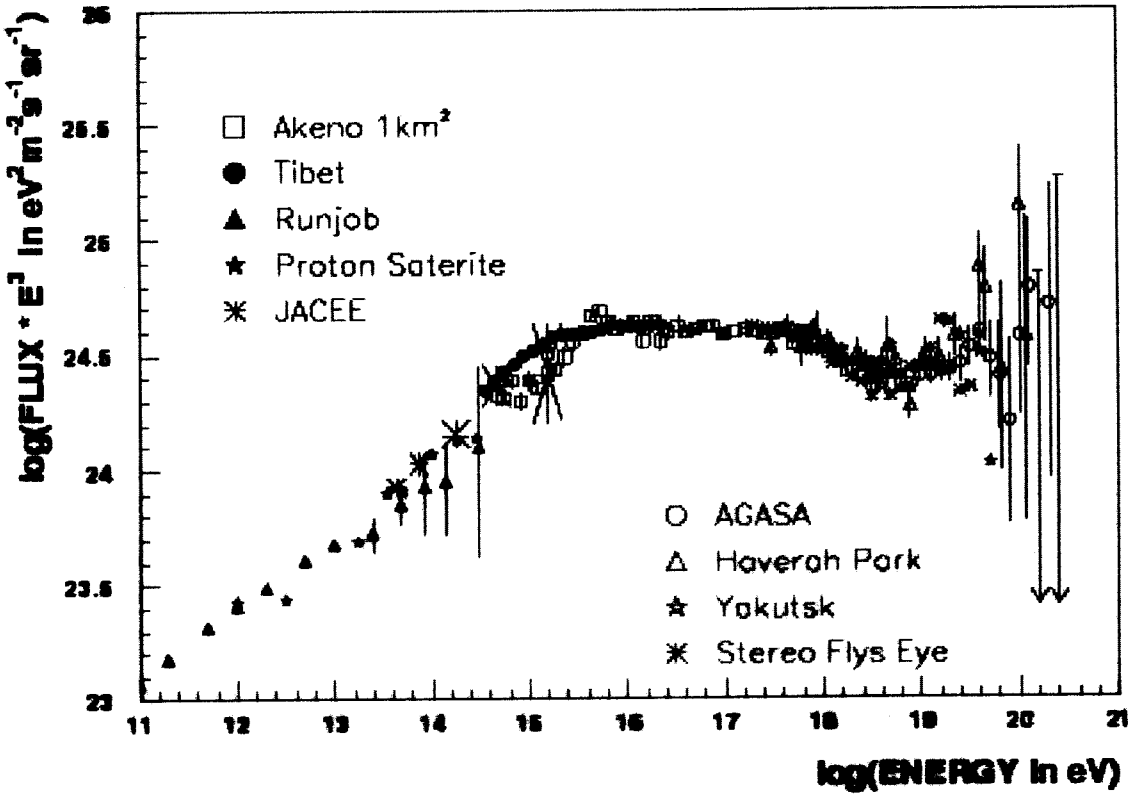

Cosmic ray flux scaled by E^3

- **Structure in a power law spectrum:**
  1. *knee* at $\sim 4 \times 10^{15}$eV
  2. second *knee* at $\sim 4 \times 10^{17}$eV
  3. *ankle* $\sim 4 \times 10^{18}$eV
  4. *cutoff* at $\sim 10^{20}$eV ... or not!

3. New results (con't) ...

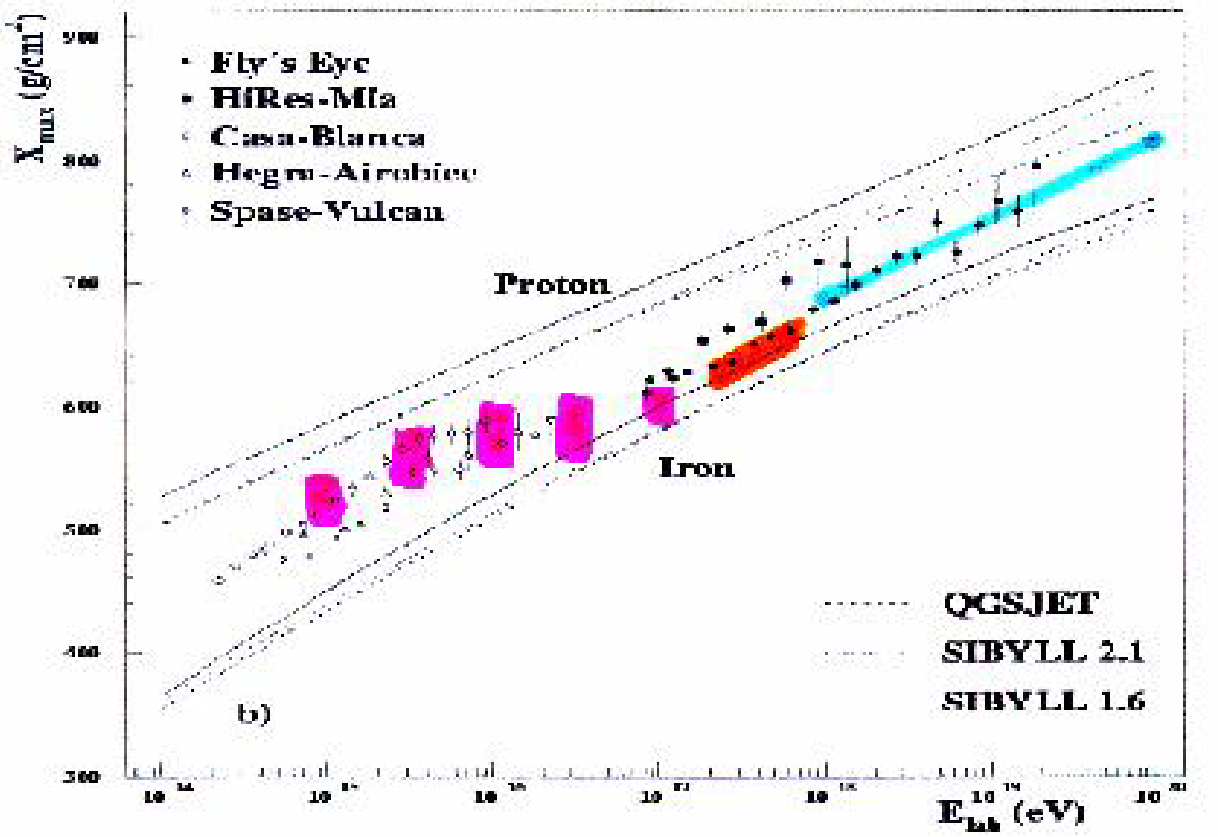

Cosmic ray *composition* including new results

- **Average depth of shower maximum (X_{max}) is sensitive to primary cosmic ray *composition*:**
  1. *red* - KASKADE (preliminary): astro-ph/0201109
  2. *orange* - Haverah Park (re-analyzed): astro-ph/0203150, consistent with *mixed* composition [34%-light (p), 66%-heavy (Fe)]
  3. *blue* - HiRes (preliminary): K. Reil, Thesis, March 2002

Pierre Sokolsky, SPIE, August 2002

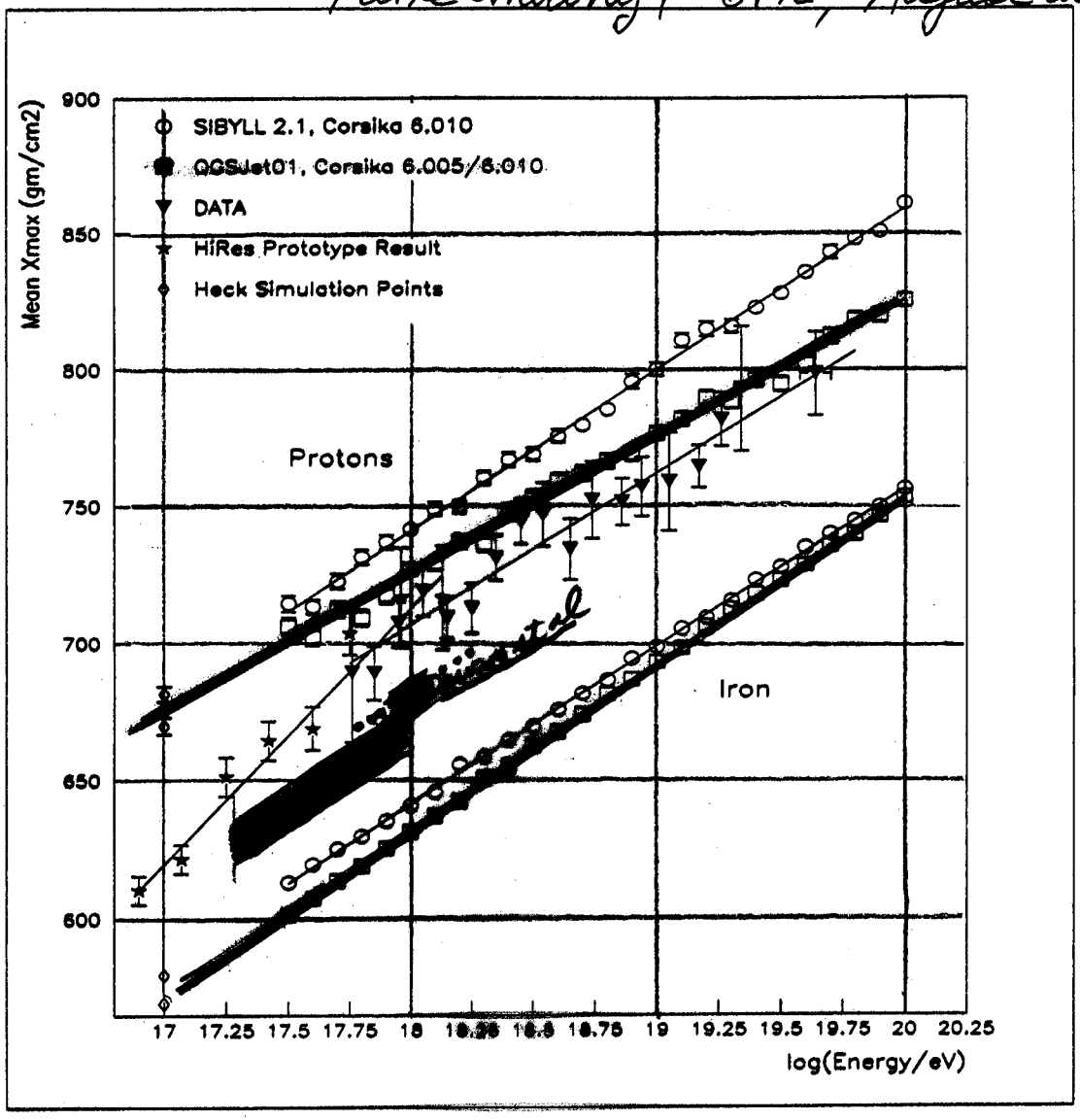

Fig. 9. Elongation Rate of HiRes stereo data set (triangles) and HiRes prototype/MIA data (stars). Open symbols show expected elongation rate for pure proton or pure Fe flux for two models of the hadronic interactions as implemented in CORSIKA.

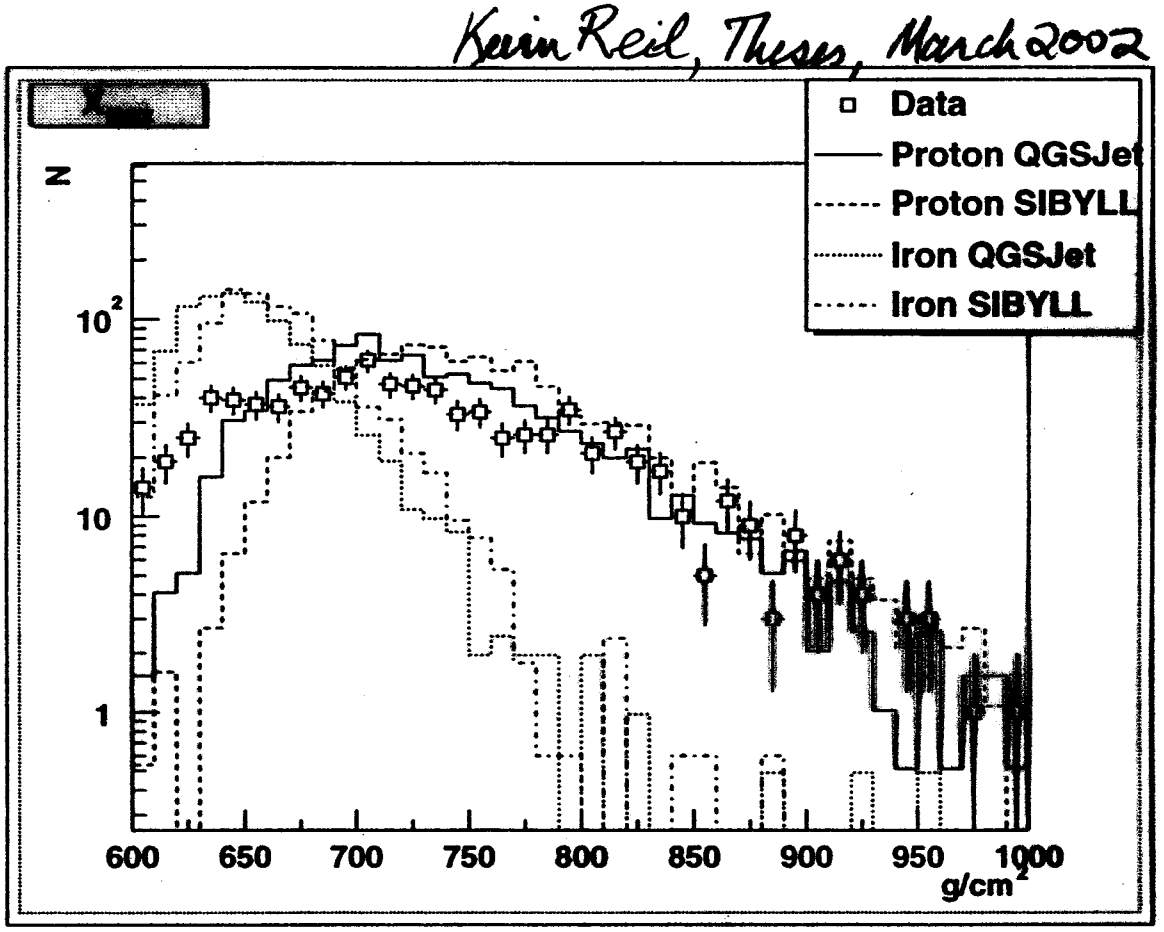

Figure 7.26. X_{max} Distribution

4. Emerging model (con't) ... *Simple* summary

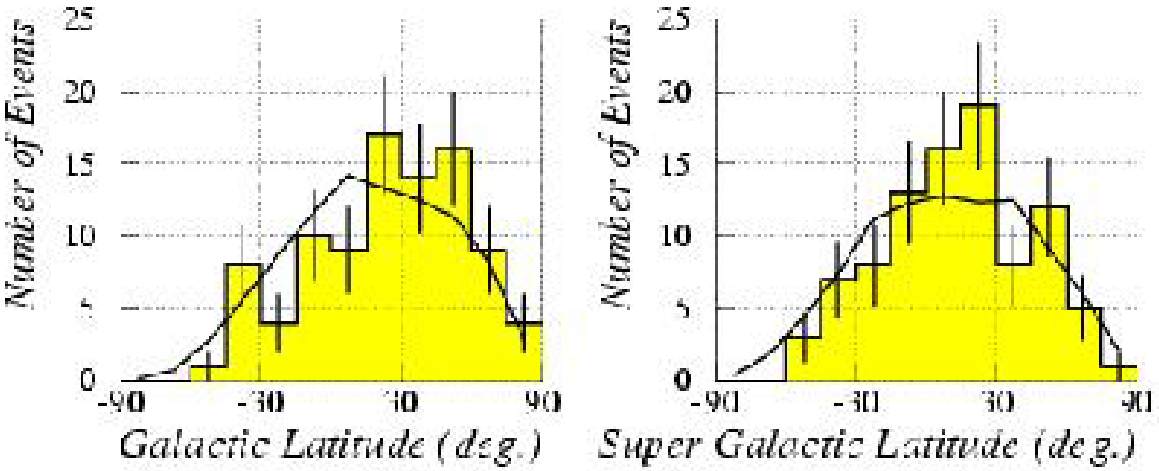

Cosmic ray ($> 4 \times 10^{19}$eV) arrival directions ...

1. 1^{st} component: broad *composition* light (p,He) to heavy (Si,Fe,..); may extend to energies $\sim 10^{19}$eV
2. 2^{nd} component: lighter (significant proton) composition; possibly measurable implications to below 10^{18}eV
3. **Primary motivations for the 2^{nd} component**: **flattening** of the flux above the ankle ($\sim 4 \times 10^{18}$eV) and a **change to lower mass composition** at the highest cosmic ray energies: above $\sim 10^{18}$eV
4. The primary motivation for identifying the 2^{nd} component as **extra-galactic** is the **isotropy of the highest energy cosmic rays** (strengthened if *light* (p,He))

D. De Marco, P. Blasi & A. Olinto, Jan 2003.

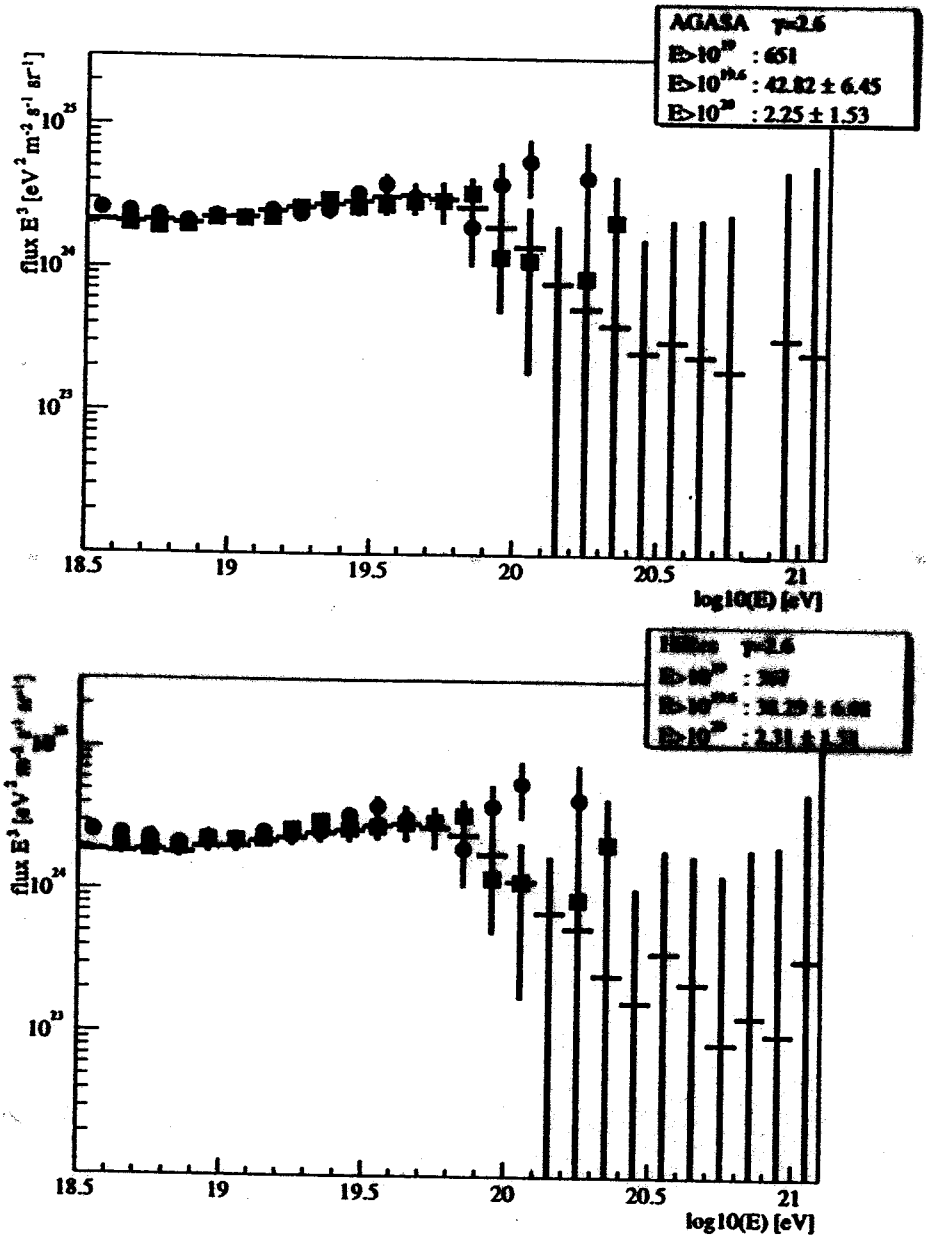

Fig. 7. Upper panel: AGASA (grey dots). lower panel: HiResI (dark squares)

... and extragalactic models should be compared to $f_p * \Phi$ where f_p is the fraction "P/all" VS energy.

B. Wiebel-Sooth & P. Biermann, Sept 1998

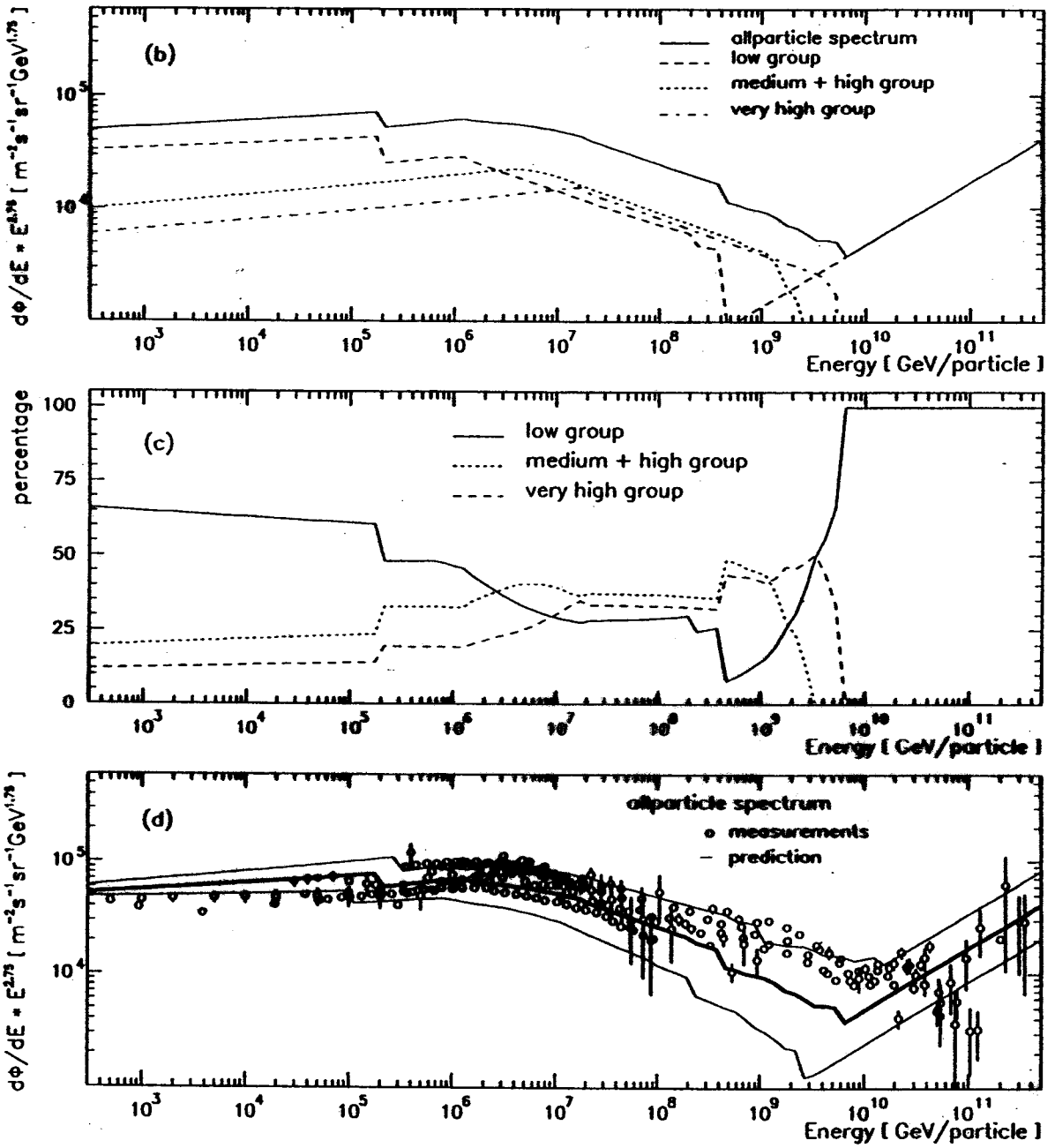

Figure 19: (a) The predicted allparticle energy spectrum (Biermann's model) with the contributions of supernovae exploding into the interstellar medium (ISM-SN), supernovae exploding into their former stellar wind (wind-SN) and radio galaxy hot spots. (b) The predicted allparticle spectrum with the contributions of several element groups. (c) The percentages of the different element groups in the allparticle flux. (d) The allparticle energy spectrum measured by the different experiments so far, with the predicted allparticle spectrum shown in (a) (thick solid line) and the error range including errors inherent in the theory (thin solid lines). Concerning the extragalactic component (radio galaxy hot spots) losses coming from interactions with the microwave background above roughly $3 \cdot 10^{10}$ GeV have been ignored here.

Design Report March 1997

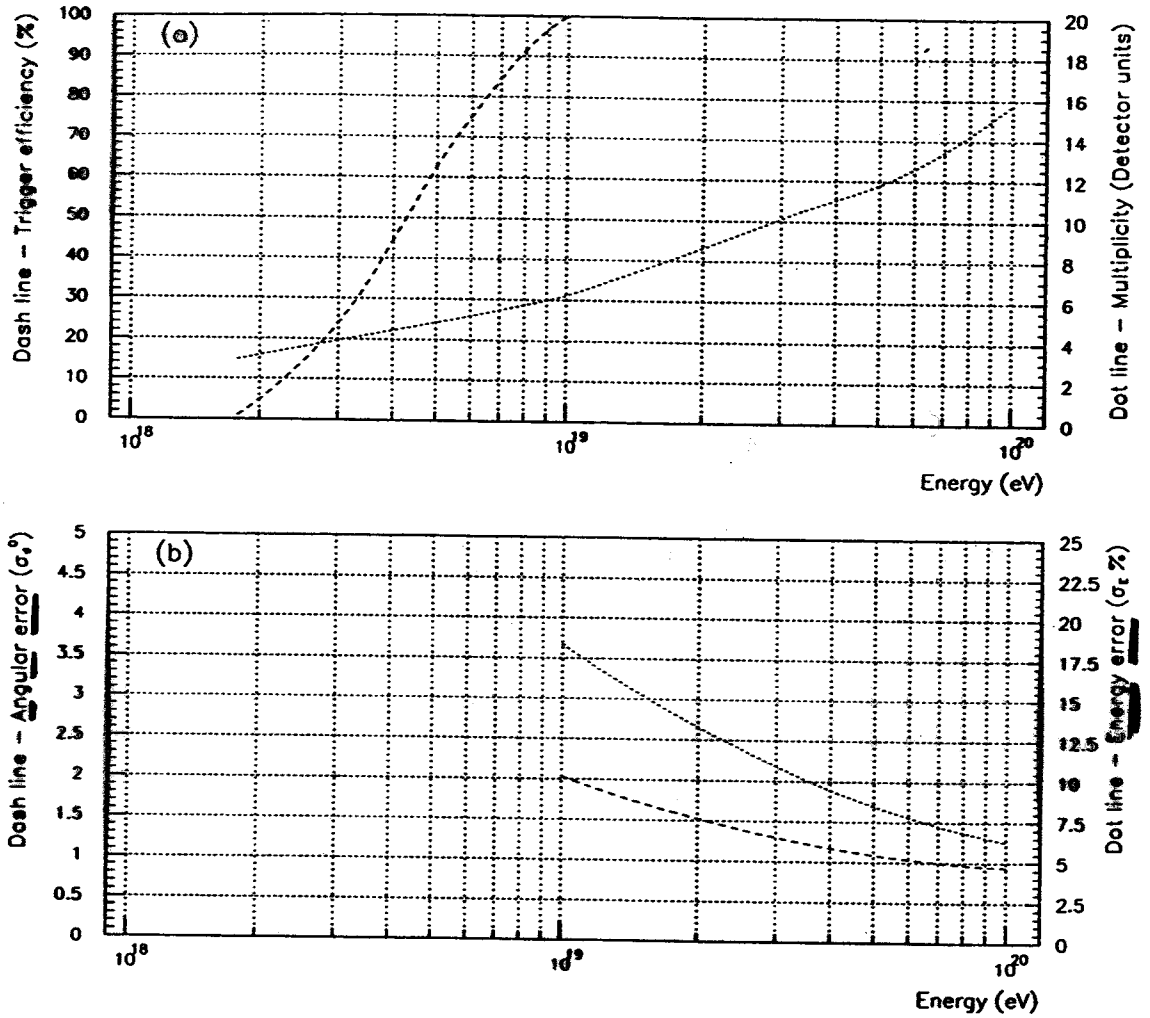

Figure 5.15: Summary of Auger Observatory water Čerenkov surface array performance as determined by reconstruction of simulated events. The upper plot shows the detector unit multiplicity and array trigger efficiency if 5 fold events are demanded, for proton showers at 30° (complete to last figure which used vertical showers). In the lower plot, expected reconstruction accuracy of direction and energy for vertical proton showers. The energy error plotted is only the random component due to detector physics and statistics. The estimated shower-to-shower fluctuations contribute 10% to the energy resolution, which should be added in quadrature with the values shown. The assumption of primary particle type results in a systematic shift of at most 25%. This systematic shift can be substantially corrected using rise time measurements, muon counting, and X_{max} measurements. The corrections can be calibrated and confirmed using hybrid data.

Design Report March 1997

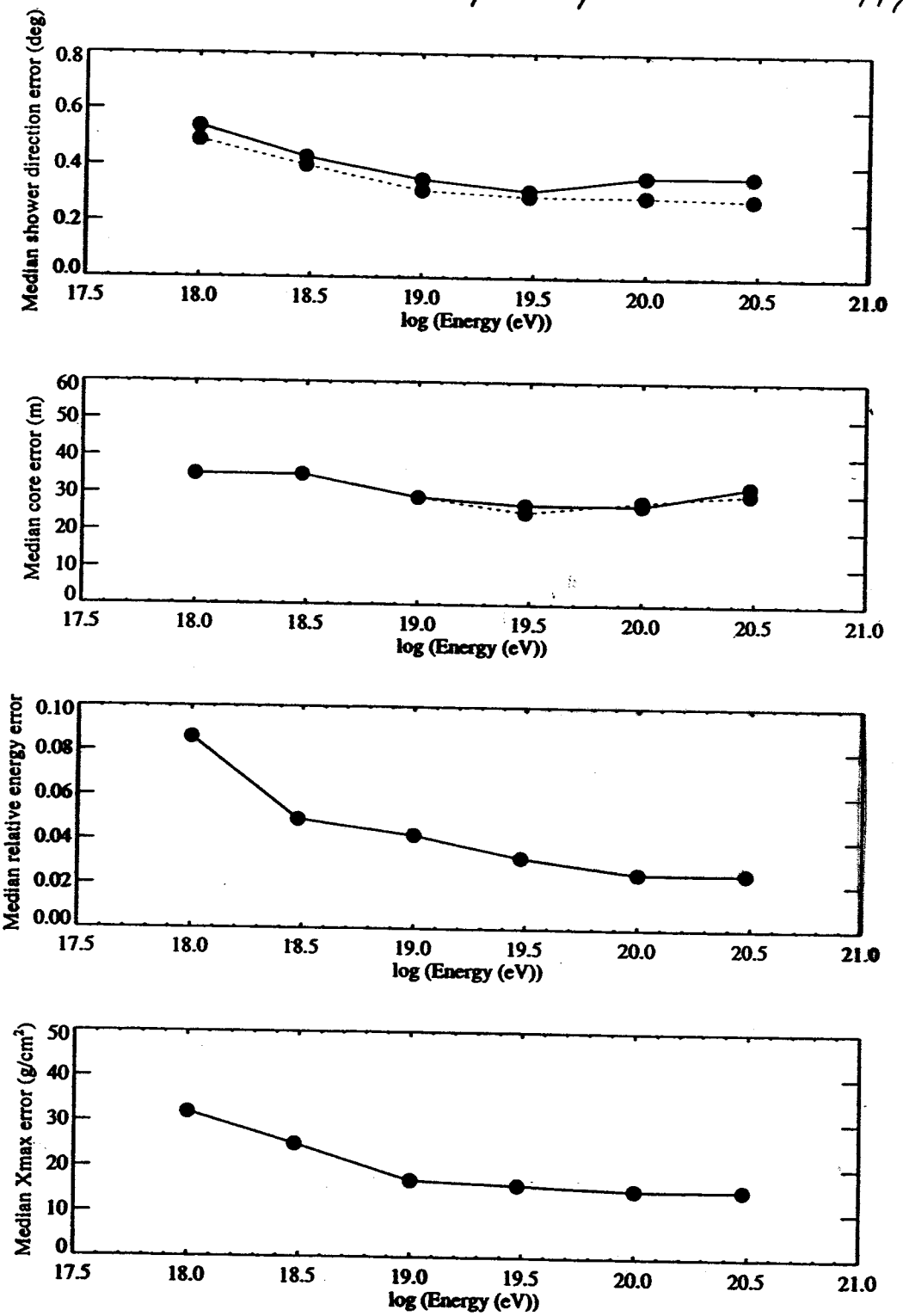

Figure 5.27: Hybrid median reconstruction errors for the three eye, 1.5° pixel system. The errors for the geometical quantities (shower direction and core) are shown for Methods 2 (solid line) and 3 (dashed line), though the errors are almost identical. The energy and X_{max} errors are shown for Method 2. A summary of these data, together with 90% errors, is given in Table 5.2.

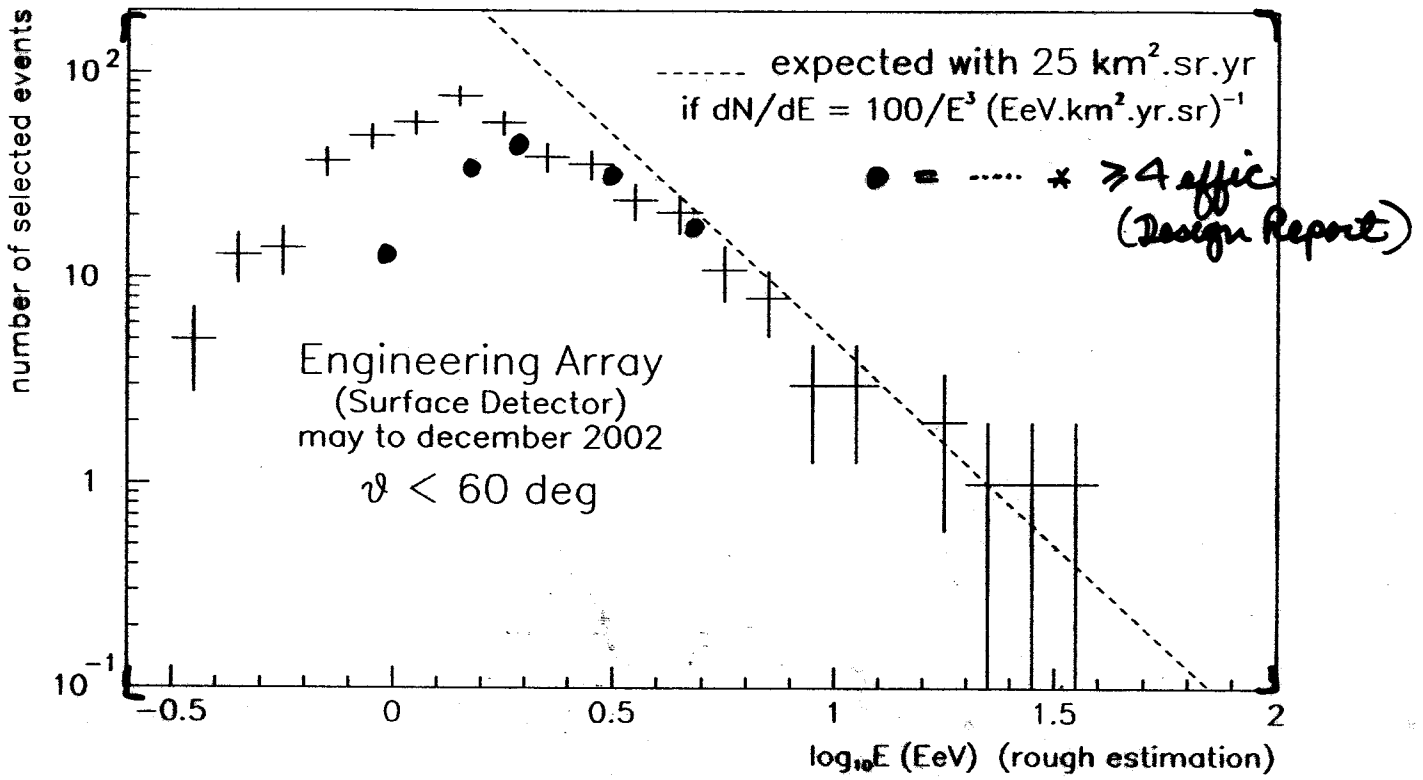
number of selected events
10^2
10
1
10^{-1}
----- expected with 25 km².sr.yr
if dN/dE = 100/E³ (EeV.km².yr.sr)⁻¹
● = ····· * ⩾4 offic
(Design Report)
Engineering Array
(Surface Detector)
may to december 2002
$\vartheta < 60$ deg
−0.5
0
0.5
1
1.5
2
$\log_{10}$E (EeV) (rough estimation)

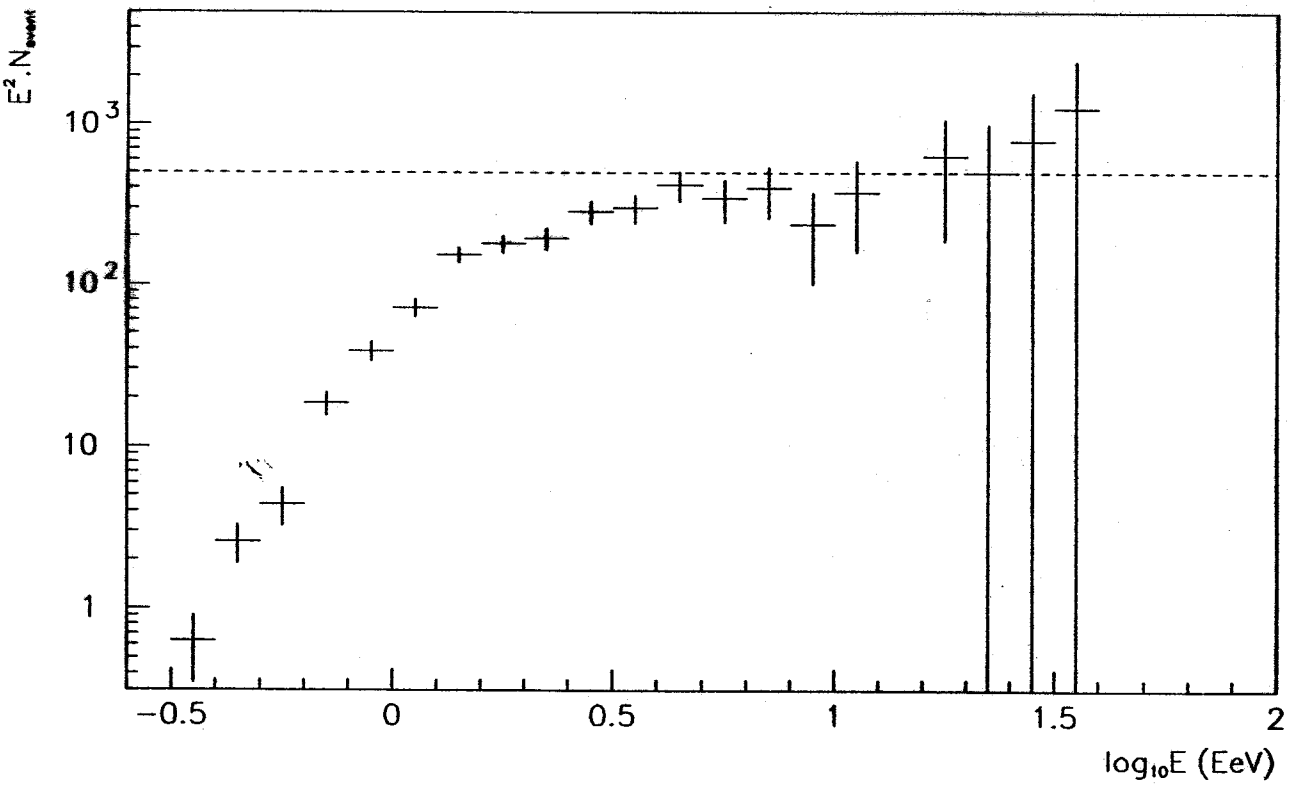
$E^2.N_{event}$
10^3
10^2
10
1
−0.5
0
0.5
1
1.5
2
$\log_{10}$E (EeV)